Flexible Coupler Array With Reconfigurable Pattern: Mechanical Beamforming and Digital Agent

Xiaodan Shao, *Member, IEEE*, Yixiao Zhang, *Graduate Student Member, IEEE*, Nan Cheng, *Senior Member, IEEE*, Weihua Zhuang, *Fellow, IEEE*, and Xuemin Shen, *Fellow, IEEE*

***Abstract*—This paper proposes a novel flexible coupler antenna array that incorporates additional degrees of freedom (DoF) in radiation pattern reconfiguration to achieve strong mechanical beamforming gains and enhanced communication coverage with low hardware cost. Particularly, passive couplers move around a fixed active antenna so that the induced currents on the passive elements can be reshaped to achieve radiation pattern reconfiguration. A new form of mechanical beamforming can be obtained by moving only the passive couplers while keeping the active antenna stationary. In addition, the flexible coupler antenna can slide along a rail toward users, thereby enhancing communication coverage. To fully exploit the potential of the flexible coupler array, we formulate a two-timescale sum-rate maximization problem with statistical channel state information (CSI). The active antenna position is optimized based on scattering cluster-core statistics in the slow timescale, while mechanical beamforming is optimized based on multipath channel statistics in the fast timescale, subject to movement and energy constraints. To address the coupling between timescales and the high cost of extensive channel sampling, we develop a digital agent framework that leverages an electromagnetic (EM) map to generate statistical channel information for different user and antenna positions. Then, a deep neural network is trained to learn a slow-fast performance (SFP) surrogate, which is fine-tuned with a small number of real measurements and then applied for position optimization at the slow timescale using projected gradient ascent. Mechanical beamforming at the fast timescale is obtained by selecting per-antenna radiation patterns from a predefined dictionary via a convex relaxation. Simulation results demonstrate that the proposed flexible coupler array significantly improves system throughput, and the digital agent-assisted algorithm achieves satisfactory performance with greatly reduced online computational complexity.**

***Index Terms*—Flexible coupler antenna (FCA) array, mechanical beamforming, antenna and coupler position optimization, reconfigurable antenna pattern, digital agent, deep learning.**

I. Introduction

MULTIPLE-INPUT multiple-output (MIMO) communication technology will remain pivotal for future sixth-generation (6G) and beyond, where the demand for massive connectivity, ultra-low latency, and high energy efficiency is driving the exploration of advanced wireless communication technologies. The MIMO technology achieves these goals through spatial multiplexing, high beamforming gains, and multi-user communications [1], [2], [3], [4], [5], [6]. An appealing feature of MIMO is that its performance gains scale with the number of antennas. As MIMO dimensions increase, however, it inevitably amplifies critical system-level challenges, including steadily increasing signal processing overhead, hardware cost, and computational complexity [7], [8]. Moreover, since the antennas in conventional MIMO systems are deployed at fixed positions, the system lacks the capability to adaptively reconfigure the wireless channel within the transmit-receive region in response to the user distribution and the environmental dynamics [9]. Therefore, it is desirable to enable flexible allocation of antenna resources in accordance with the spatially nonuniform distribution of users to enhance their performance gains.

To fully exploit spatial channel variations, the novel six-dimensional movable antenna (6DMA) has recently been proposed to increase MIMO system capacity without requiring additional antennas [10], [11], [12]. This technique leverages the adaptability of antenna positions and rotations (i.e., orientations) in three-dimensional (3D) space at transceivers to adaptively allocate antenna resources based on the spatial distribution of channels. In [13], the authors proposed a six-dimensional movable holographic surface-assisted integrated data and energy transfer system. In [14], low-training-complexity channel estimation algorithms were proposed by exploiting a new directional-sparsity characteristic of 6DMA channels. Then, a 6DMA-enabled wideband terahertz (THz) communication system with a sub-connected hybrid beamforming architecture was studied in [15]. The authors in [16] investigated a new unmanned aerial vehicle (UAV)-enabled passive 6DMA architecture. The authors in [17] discussed two special cases of 6DMA, namely a rotatable antenna with fixed position and a translatable antenna with fixed rotation. Other studies also explored 6DMA-enhanced integrated sensing and communications (ISAC) [18], polarized 6DMA [19], and fluid antenna systems [20]. Despite its promising applications, the existing 6DMA designs move the active antenna element

Received 12 January 2026; revised 1 April 2026; accepted 30 April 2026. Date of publication 12 May 2026; date of current version 15 May 2026. This work was supported by research grants from the Natural Sciences and Engineering Research Council (NSERC) of Canada. The associate editor coordinating the review of this article and approving it for publication was A. Kaushik. *(Corresponding authors: Xuemin Shen; Weihua Zhuang.)*

Xiaodan Shao, Yixiao Zhang, Weihua Zhuang, and Xuemin Shen are with the Department of Electrical and Computer Engineering, University of Waterloo, Waterloo, ON N2L 3G1, Canada (e-mail: x6shao@uwaterloo.ca; y3549zha@uwaterloo.ca; wzhuang@uwaterloo.ca; sshen@uwaterloo.ca).

Nan Cheng is with the State Key Laboratory of ISN, School of Telecommunications Engineering, Xidian University, Xi'an 710071, China (e-mail: nancheng@xidian.edu.cn).

Digital Object Identifier 10.1109/TCOMM.2026.3692017

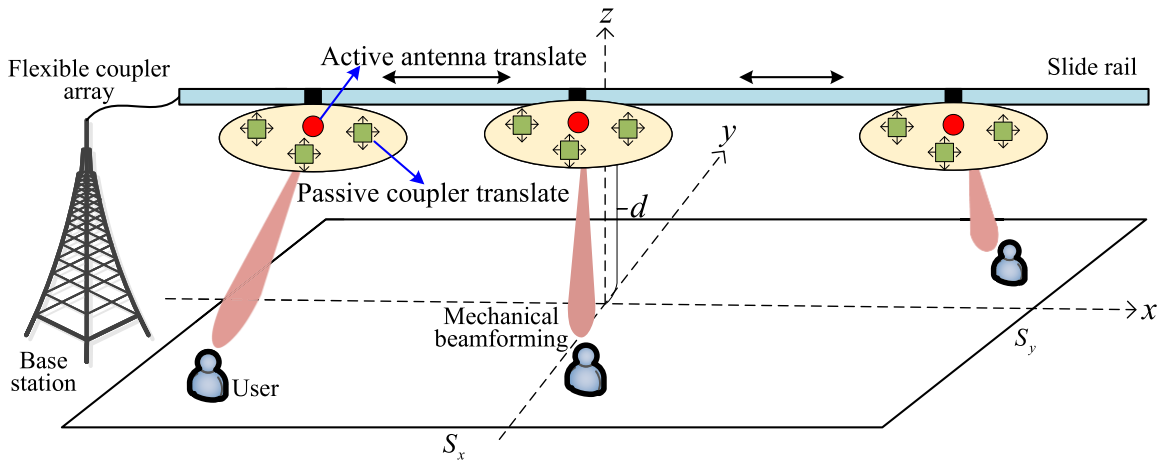

Fig. 1. Illustration of flexible coupler antenna array for mitigating large-scale path loss and enabling mechanical beamforming.

together with its radio-frequency (RF) feed over a sufficiently large region with a size on the order of several to tens of wavelengths to exploit spatial channel variations, which introduces substantial mechanical complexity and energy consumption.

Fortunately, the authors in [21] proposed a low-complexity flexible coupler antenna, where mutual coupling can serve as an enabler of advanced spatial processing to improve system performance. By dispensing with the requirement that each antenna be connected to a dedicated RF chain, each flexible coupler antenna is connected to a single RF chain and multiple passive couplers [21], [22]. By rotating or shifting only passive couplers within a small area via electromagnetic (EM) coupling, the induced coupling currents can be reshaped to enhance communication performance without moving the active antenna or the associated RF hardware [21], [22]. However, existing flexible coupler antennas typically permit coupler translations on the order of several wavelengths. Such constraints hinder the mitigation of large-scale path loss and consequently restrict communication performance. Moreover, optimization and channel estimation for flexible antenna systems mainly rely on real-world data measurements. As the number of antennas and antenna reconfigurable parameters increases, exhaustive testing in physical environments becomes infeasible given the ultra-low latency requirements of future wireless systems.

To address these challenges, we first design a flexible coupler array that combines the small-range relocation of passive couplers with large-scale active antenna translation, as shown in Fig. 1. Then, we introduce digital agent, which is conceptually related to that of the digital twin [23], [24]. It replicates physical assets in a digital space for testing and analysis without interfering with the real system. Unlike digital twins in manufacturing [25], which primarily focus on monitoring and offline simulation, an antenna digital agent emphasizes modeling network behavior, learning the characteristics of the radio environment, and enabling real-time configuration as well as customized network management. As a practical implementation of a digital agent, the EM map, also referred to as the channel knowledge map, has been proposed [26]. It is a site-specific database tagged with the locations of transmitters and receivers, containing channel-related information useful to enhance environment-awareness and facilitate or even obviate sophisticated real-time channel state information (CSI) acquisition. Unlike conventional channel knowledge maps that aim to predict instantaneous channel realizations, the EM map considered in this paper stores slowly varying statistical channel information derived from environmental geometry, antenna parameters, and user positions, which reduces the overhead of channel reconstruction. In this way, the digital agent can provide reliable statistical CSI and performance surrogates under stringent latency constraints, thereby supporting efficient antenna position optimization and mechanical beamforming in flexible coupler systems. In practice, the proposed flexible coupler array with digital agent can be deployed in different applications. For example, a slide rail can be mounted along the wall of a subway station, where the digital agent uses the EM map to track user flows along the platform and adapt active antenna positions and radiation patterns to overcome strong blockage by pillars, thereby maintaining coverage.

The main contributions of this paper are summarized as follows.

- We propose the *flexible coupler antenna* that moves *passive* couplers around an active antenna, where passive-coupler position variations induce mechanical beamforming for radiation pattern reconfiguration. The flexible coupler antenna can also slide along a rail to move close to the receiver, thereby establishing a strong communication link and mitigating large-scale path loss. Here, the active antenna moves over a much larger range along the rail, whereas the passive couplers only perform local wavelength-scale adjustments around the active antenna. Mechanical beamforming enables a reconfigurable radiation pattern that extends angular coverage, which reduces the number of required slide rails and the hardware cost for achieving full spatial coverage. Moreover, moving passive couplers instead of the active antenna avoids moving RF hardware, thus providing fine beam-steering capability while reducing mechanical complexity.

- We formulate an optimization problem to maximize the user sum rate by jointly designing the mechanical beamformer and the active-antenna position vector based on channel statistics. To solve the problem, we develop a digital agent-assisted two-timescale optimization framework for flexible coupler array. At the fast timescale, the mechanical beamformer is optimized to maximize the ergodic sum rate under statistical CSI by convex relaxation. At the slow timescale, we extract statistical CSI from an EM map to train a slow-fast performance (SFP) surrogate with a deep neural network for predicting the optimized sum rate as a function of the active-antenna position vector, which already accounts for the fast-timescale mechanical-beamforming optimization. The surrogate is further fine-tuned online and used to update active antenna position by a single projected gradient step. The proposed design avoids repeated fast-timescale mechanical beamforming during position optimization, reduces online complexity, and removes the need for explicit prior knowledge of the instantaneous channel.
- Extensive simulations are conducted to validate the capability of the proposed flexible coupler array to enhance system performance, as well as the effectiveness of the proposed digital-agent-aided two-timescale algorithm in reducing online computational complexity and adapting to changing environments.

The rest of this paper is organized as follows. Section II presents the flexible coupler array together with the corresponding channel and signal models. Section III introduces the slow and fast timescale protocol for the flexible coupler system and formulates the sum rate maximization problem by jointly designing mechanical beamforming and active antenna positions under practical constraints. Section IV describes the digital agent-aided algorithm for active antenna position and mechanical beamforming design. Section V discusses numerical results for performance evaluation and comparison. Finally, Section VI concludes this study.

Notations: Boldface upper-case and lower-case letters denote matrices and vectors, respectively, $(\cdot)^H$ and $(\cdot)^T$ respectively denote conjugate transpose and transpose, and $\mathbb{E}[\cdot]$ denotes the expected value of a random variable. For a scalar a, $|a|$ denotes its magnitude. For a vector $\mathbf{a}$, $\|\mathbf{a}\|_2$ and $\|\mathbf{a}\|_1$ denote the ℓ_2-norm and ℓ_1-norm, respectively. Operator $\mathrm{diag}(\mathbf{x})$ denotes a diagonal matrix with the diagonal entries specified by vector $\mathbf{x}$, $[\mathbf{a}]_j$ denotes the j-th element of vector $\mathbf{a}$, $[\mathbf{A}]_{i,j}$ denotes the element of matrix $\mathbf{A}$ at the i-th row and j-th column, $\otimes$ denotes the Kronecker product, $\mathbf{I}_M$ denotes an $M \times M$ identity matrix, $\mathrm{blkdiag}\{\mathbf{A}_1, \mathbf{A}_2, \ldots, \mathbf{A}_M\}$ denotes a block diagonal matrix, $\mathrm{vec}(\mathbf{A})$ denotes the vectorization operator that stacks all the columns of a matrix $\mathbf{A}$ into a single column vector, $\mathcal{O}(\cdot)$ denotes the big-O notation, $\mathbb{R}$ and $\mathbb{C}$ denote the real and complex fields, respectively, $\mathcal{N}(\mu, \sigma^2)$ denotes a real Gaussian distribution with mean μ and variance σ^2, and $\mathcal{CN}(\boldsymbol{\mu}, \boldsymbol{\Sigma})$ denotes a circularly symmetric complex Gaussian distribution with mean $\boldsymbol{\mu}$ and covariance matrix $\boldsymbol{\Sigma}$.

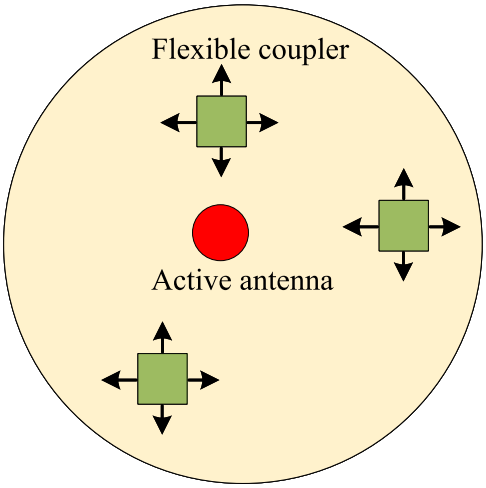

Fig. 2. Top view of the flexible coupler antenna with reconfigurable coupler position.

II. System Model

We consider an uplink system where a base station (BS) serves a set of single-antenna users $\mathcal{K} = \{1, \ldots, K\}$, with K denoting the total number of users. As illustrated in Fig. 1, the BS is equipped with a flexible coupler array, where N flexible coupler antennas are mounted on one slide rail, and each flexible coupler antenna can move along the slide rail on a scale much larger than a wavelength and can be positioned close to users to form a strong communication link. The slide rail is installed at a fixed height of d and aligned parallel to the x-axis. As shown in Fig. 2, each flexible coupler antenna consists of one fixed-position active antenna and multiple passive couplers that move within a designated area around the active antenna [21], [22]. The positions of the passive couplers can be mechanically adjusted with the aid of drive components such as micro-electromechanical systems (MEMS), which provide low power consumption and fast response [22]. Each passive coupler is modeled as a thin straight-wire dipole. The active antenna is connected to a single RF chain, and the receiver is assumed to have a fixed single antenna. By moving the passive couplers around the fixed active radiator, the antenna's radiation pattern is reconfigured through the induced currents on the passive coupler without moving the active antenna's RF chains [21].

The users are distributed within a known two-dimensional area, e.g., a rectangular region with a size of $S_x \times S_y$ m^2. The location of the active antenna in the n-th flexible coupler antenna on the slide rail in the Cartesian coordinate system is given by $[p_n, 0, d]$, where $0 \leq p_n \leq X$ denotes the position of the active antenna on a slide rail of length X.

A. Mechanical Beamforming

We refer to the capability of steering and shaping the EM radiation pattern by mechanically relocating the passive coupler elements around the fixed active antenna as mechanical beamforming [21]. In mechanical beamforming, the beam direction and beam shape are controlled through the geometry and positions of the passive couplers, while the RF chains of the active antenna remain fixed.

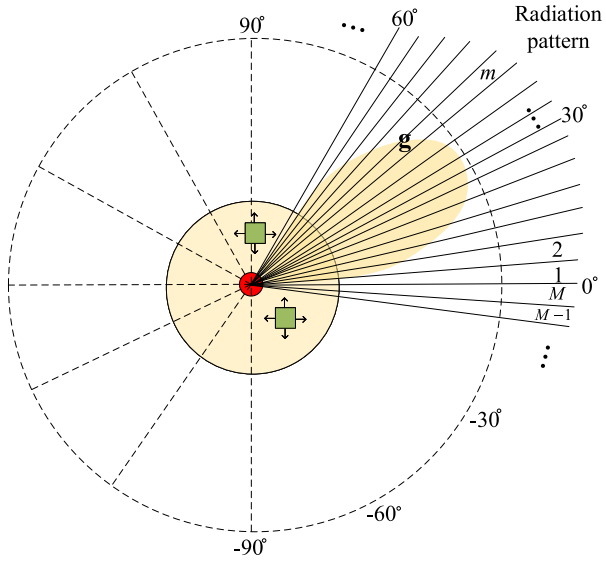

Fig. 3. Reconfigurable antenna pattern for flexible coupler antenna.

To quantify the performance gains enabled by mechanical beamforming with flexible couplers, we establish a mathematical model for the radiation pattern and the associated channel characteristics. The flexible coupler introduces an additional DoF in the angular domain, which expands the information coverage of a conventional antenna from a one-dimensional spatial representation to an M-dimensional angular representation, where M is the number of uniformly sampled directions. The reconfigurable radiation pattern in the angular domain is therefore characterized over M discrete angular directions (see Fig. 3). To model reception characteristics, we introduce the virtual angular-index channel for any flexible coupler antenna, denoted as

$$z \in \{0,1\}^M, \tag{1}$$

which serves as an index vector indicating the spatial angles at which the user is located.

Let $\mathbf{q}_n$ denote the position vector of the passive couplers in the n-th flexible coupler antenna. Since the radiation pattern is determined by the relative geometry between the active antenna and passive couplers, the resulting pattern of the n-th flexible coupler antenna in the EM angular domain can be represented as a function of $\mathbf{q}_n$, denoted by

$$\mathbf{g}_n(\mathbf{q}_n) \in \mathbb{R}^M, \tag{2}$$

with each element corresponding to the radiation gain in one of the M discrete directions. Consequently, the effective gain of the n-th flexible coupler antenna in the EM angular domain can be written as

$$B_n = z^T \mathbf{g}_n(\mathbf{q}_n), \tag{3}$$

which quantifies the radiation intensity directed toward the user's actual spatial angle. By optimizing the radiation pattern $\mathbf{g}_n(\mathbf{q}_n)$ to align with the angular-domain channel characteristics $\mathbf{z}$, their correlation and thus the effective radiation efficiency, B_n, is maximized. This formulation serves as the foundation for the following theoretical analysis and optimization.

Building upon the radiation pattern model of a single flexible coupler antenna presented above, we extend this model to characterize the programmable radiation pattern of the entire flexible coupler array at the BS, which consists of N flexible coupler antennas. The resulting mechanical beamforming (also called radiation beamforming) in the EM angular domain is expressed in the following matrix form

$$\mathbf{G}(\mathbf{q}) \triangleq \text{blkdiag}\{\mathbf{g}_1(\mathbf{q}_1), \ldots, \mathbf{g}_N(\mathbf{q}_N)\} \in \mathbb{R}^{MN \times N}, \tag{4}$$

where the m-th element of $\mathbf{g}_n(\mathbf{q}_n)$ represents the radiation gain of the n-th flexible coupler antenna in the m-th angular direction. To ensure fairness in pattern design, the total energy of each antenna's radiation pattern is normalized as $\|\mathbf{g}_n(\mathbf{q}_n)\|^2 = 1,\ \forall n$.

To further characterize the spatial mapping of the flexible couplers, we introduce the virtual angular-index channel

$$\bar{\mathbf{Z}}_k \triangleq \text{blkdiag}\{\mathbf{Z}_{k,1}, \ldots, \mathbf{Z}_{k,N}\} \in \{0,1\}^{MN \times L_k N}, \tag{5a}$$

$$\mathbf{Z}_{k,n} \triangleq \left[z_{k,n,1},\, z_{k,n,2}, \ldots, z_{k,n,L_k}\right] \in \{0,1\}^{M \times L_k}, \tag{5b}$$

where $\mathbf{Z}_{k,n}$ specifies the spatial angles associated with the n-th flexible coupler antenna and the k-th user. Each column $\mathbf{z}_{k,n,l} \in \{0,1\}^M$ contains exactly one nonzero entry, indicating the angular direction of the l-th ($l \in \{1,2,\cdots,L_k\}$) propagation path on the n-th flexible coupler antenna for user k, with L_k being the number of propagation paths. Consequently, radiation gain $\mathbf{B}_k \in \mathbb{R}^{L_k N \times N}$ of all flexible coupler antennas toward the k-th user can be formulated as

$$\mathbf{B}_k = \bar{\mathbf{Z}}_k^T\, \mathbf{G}(\mathbf{q}) = \text{blkdiag}\big\{\mathbf{Z}_{k,1}^T \mathbf{g}_1,\, \ldots,\, \mathbf{Z}_{k,N}^T \mathbf{g}_N\big\}. \tag{6}$$

In summary, matrices $\mathbf{G}(\mathbf{q})$ and $\bar{\mathbf{Z}}_k$ mathematically capture the additional DoF introduced by flexible coupler array, enabling a more flexible and adaptive radiation beamforming strategy in the EM angular domain. Note that active-antenna position vector $\mathbf{p} = [p_1, p_2, \cdots, p_N]^T$ and mechanical beamforming vector $\mathbf{G}(\mathbf{q})$ are the design parameters that we tune to optimize the flexible coupler system throughput.

Remark 1: Unlike prior 6DMA designs that steer beams only by moving the *active* antenna [10], the proposed flexible coupler array supports dual motion, where the active antenna translates over a large range along the slide rail, while the passive couplers in each flexible coupler antenna move locally around it in the reactive near field. The induced currents on the passive couplers reshape the radiation pattern, thereby yielding fine angular resolution with much lower mechanical and RF complexity [21].

B. Channel Model

Due to the sparse scattering characteristics of wireless channels at high frequencies, e.g., millimeter-wave (mmWave) bands, the channel typically consists of a few dominant clusters, each containing multiple propagation paths [27]. Let C_k denote the total number of scattering clusters for user k, and $L_{c,k}$ denote the number of multipaths in cluster c for

user k. Then, the near-field channel between the n-th flexible coupler antenna and the k-th user can be expressed as

$$h_{k,n}(p_n)=\sum_{c=1}^{C_k}\sum_{l_c=1}^{L_{c,k}}\frac{\alpha_{k,c,l_c}}{r_{c,l_c,n}(p_n)\,r_{k,c,l_c}}e^{-j\frac{2\pi}{\lambda}\left(r_{c,l_c,n}(p_n)+r_{k,c,l_c}\right)}, \tag{7}$$

where λ denotes the carrier wavelength, $\alpha_{k,c,l_c}\in\mathbb{C}$ is the complex scattering coefficient associated with the (c,l_c)-th path for user k, r_{k,c,l_c} is the distance from user k to the l_c-th scatterer in cluster c, and $r_{c,l_c,n}(p_n)$ is the distance from that scatterer to the n-th flexible coupler antenna located at position p_n on the sliding rail.

The distance, $r_{c,l_c,n}$, can be described as

$$r_{c,l_c,n}=\bar{r}_{c,n}+\Delta r_{l_c,n}, \tag{8}$$

where $\bar{r}_{c,n}$ denotes the nominal distance from the c-th cluster center to the n-th candidate position on the slide rail, and $\Delta r_{l_c,n}$ denotes the deviation of the l_c-th ray from the cluster nominal center, following a Gaussian distribution

$$\Delta r_{l_c,n}\sim\mathcal{N}(0,\varsigma_{n,c}^2), \tag{9}$$

with $\varsigma_{n,c}^2$ indicating the distance spread. Similarly, r_{k,c,l_c} can be described as

$$r_{k,c,l_c}=\bar{r}_{k,c}+\Delta r_{k,l_c}, \tag{10}$$

where $\bar{r}_{k,c}$ denotes the nominal user-cluster distance for the c-th scattering cluster and user k, and $\Delta r_{k,l_c}$ denotes the corresponding deviation, following a Gaussian distribution

$$\Delta r_{k,l_c}\sim\mathcal{N}(0,\iota_{k,c}^2), \tag{11}$$

with $\iota_{k,c}^2$ indicating the distance spread.

For clarity, we define $L_k\triangleq\sum_{c=1}^{C_k}L_{c,k}$ as the total number of paths. With this notation, the near-field spatial channel coefficient between the n-th flexible coupler antenna and the k-th user in (7) can be reformulated as

$$h_{k,n}(p_n)=\sum_{l=1}^{L_k}\frac{\alpha_{k,l}}{r_{l,n}(p_n)\,r_{k,l}}e^{-j\frac{2\pi}{\lambda}\left(r_{l,n}(p_n)+r_{k,l}\right)}. \tag{12}$$

Furthermore, the integration of the reconfigurable pattern extends the channel representation from a one-dimensional to an M-dimensional formulation by incorporating additional radiation channel information, i.e., $\bar{\mathbf{Z}}_k$ in (5a). The dimension-extended channel for the n-th flexible coupler antenna, denoted by $\mathbf{h}_{k,n}(p_n)\in\mathbb{C}^M$, is given by

$$\mathbf{h}_{k,n}(p_n)=\sum_{l=1}^{L_k}\frac{\alpha_{k,l}}{r_{l,n}(p_n)\,r_{k,l}}e^{-j\frac{2\pi}{\lambda}\left(r_{l,n}(p_n)+r_{k,l}\right)}\mathbf{z}_{k,n,l}. \tag{13}$$

By stacking the channel vectors $\mathbf{h}_{k,n}(p_n)\in\mathbb{C}^M$ of all N antennas, we obtain the complete channel vector for user k as follows

$$\mathbf{h}_k(\mathbf{p})=[\mathbf{h}_{k,1}^T(p_1),\cdots,\mathbf{h}_{k,N}^T(p_N)]^T \tag{14a}$$

$$=\bar{\mathbf{Z}}_k\,\bar{\mathbf{h}}_k(\mathbf{p})\in\mathbb{C}^{MN}, \tag{14b}$$

where $\bar{\mathbf{Z}}_k$ is defined in (5a) and

$$\bar{\mathbf{h}}_k(\mathbf{p})=\mathrm{vec}\big(\mathbf{A}_k^T(\mathbf{p})\big)\in\mathbb{C}^{NL_k}, \tag{15}$$

with $\mathbf{A}_k(\mathbf{p})=[\alpha_{k,1}\,\mathbf{a}_{k,1}(\mathbf{p}),\ \ldots,\ \alpha_{k,L_k}\,\mathbf{a}_{k,L_k}(\mathbf{p})]\in\mathbb{C}^{N\times L_k}$ and $\mathbf{a}_{k,l}(\mathbf{p})=\left[\frac{e^{-j\frac{2\pi}{\lambda}(r_{l,1}(p_1)+r_{k,l})}}{r_{l,1}(p_1)\,r_{k,l}},\ \ldots,\ \frac{e^{-j\frac{2\pi}{\lambda}(r_{l,N}(p_N)+r_{k,l})}}{r_{l,N}(p_N)\,r_{k,l}}\right]^T$.

This additional positional flexibility on a scale much larger than a wavelength enables the proposed flexible coupler array to establish a stronger and more stable communication link to the user than conventional fixed-antenna systems, which lack the ability to dynamically reconfigure or reconstruct the wireless channel.

C. Signal Model

We consider the uplink transmission from K single-antenna users to the BS. The received signals at the BS are given by

$$\mathbf{y}=\mathbf{G}^H(\mathbf{q})\mathbf{H}(\mathbf{p})\mathbf{x}+\mathbf{n}, \tag{16}$$

with

$$\mathbf{H}(\mathbf{p})=[\mathbf{h}_1(\mathbf{p}),\mathbf{h}_2(\mathbf{p}),\cdots,\mathbf{h}_K(\mathbf{p})]\in\mathbb{C}^{MN\times K}, \tag{17}$$

denoting the multiple-access channel from all K users to the flexible coupler array at the BS. In (16), $\mathbf{x}=\sqrt{\rho}[x_1,x_2,\cdots,x_K]^T\in\mathbb{C}^{K\times 1}$ with x_k denoting the transmit signal of user k with the average power normalized to one, and ρ representing the transmit power of each user (assumed to be identical for all users). Vector $\mathbf{n}\sim\mathcal{CN}(\mathbf{0},\sigma^2\mathbf{I}_N)$ denotes the complex additive white Gaussian noise (AWGN) vector at the BS with zero mean and average power σ^2.

According to Shannon's formula, the achievable sum-rate of all users over unit radio spectrum bandwidth is given by

$$\begin{aligned}&R(\mathbf{p},\mathbf{G}(\mathbf{q}))\\&=\log_2\det\left(\mathbf{I}_N+\frac{1}{\sigma^2}\sum_{k=1}^{K}\rho\mathbf{G}^H(\mathbf{q})\mathbf{h}_k(\mathbf{p})\mathbf{h}_k^H(\mathbf{p})\mathbf{G}(\mathbf{q})\right)\\&=\log_2\det\left(\mathbf{I}_N+\frac{\rho}{\sigma^2}\mathbf{G}^H(\mathbf{q})\mathbf{H}(\mathbf{p})\mathbf{H}^H(\mathbf{p})\mathbf{G}(\mathbf{q})\right),\end{aligned} \tag{18}$$

in bits per second per Hertz (bps/Hz), which depends only on the set of selected active antenna positions, rather than on the specific assignment of these positions to individual antennas. It is worth noting that, in contrast to the conventional multiuser channel with fixed-position antennas, the capacity of the flexible coupler-enabled wireless channel in (18) is determined by active antenna positions $\mathbf{p}$ and mechanical beamforming (i.e., radiation beamforming) $\mathbf{G}(\mathbf{q})$.

III. Problem Formulation

A. Two Timescale Protocol With Statistical CSI

The proposed flexible coupler array encounters practical challenges, including high channel estimation overhead and considerable movement complexity. Specifically, joint optimization of active antenna positions and mechanical beamforming based on instantaneous CSI requires high-speed and frequent mechanically controlled translations, which incur substantial implementation cost and complexity. Moreover, the adjustment speed of such mechanical movements is inherently slow, so the movement duration may exceed the coherence time of the instantaneous channel, which makes instantaneous-CSI-based designs impractical.

To address this limitation, we adopt statistical CSI, under which each flexible coupler antenna moves much more slowly and less frequently to adapt to long-term channel statistics. Even under statistical CSI, the timescales of translation and mechanical beamforming must be treated hierarchically. Active antenna positions involve mechanical movements over distances much larger than the wavelength, typically from a few to several tens of meters, which limits their update speed and makes them suitable for adapting to slow-level variations, where the scattering cluster core remains nearly constant over extended periods. In contrast, the mechanical beamforming of the flexible coupler array is realized by adjusting the positions of the passive couplers via MEMS [21]. Since the couplers move only within a small range on the order of the wavelength, their positions can be rapidly adjusted to track fast-level variations, where the intra-cluster multipath statistics remain approximately stationary. Motivated by these considerations, we propose a hierarchical transmission framework that operates on scattering cluster-core statistics in the slow timescale and multipath channel statistics in the fast timescale to balance implementation feasibility and system performance, as illustrated in Fig. 4.

- **Slow timescale:** The considered time frame, T, is partitioned into T_S super-frames, denoted by $\mathcal{T}_S = \{1, 2, \ldots, T_S\}$. In each super-frame, the BS extracts cluster-core statistics (using the EM map discussed in Section IV) and optimizes the active-antenna position vector to adapt coverage to the dominant scattering-core geometry.
- **Fast timescale:** Each super-frame is further divided into T_F frames, defined as $\mathcal{T}_F = \{1, 2, \ldots, T_F\}$. In each frame, the BS acquires a statistical multipath channel within the scattering clusters to update the mechanical beamformer for enhancing array gain.

This hierarchical framework is to reduce channel estimation overhead while ensuring efficient active antenna position and mechanical beamforming adaptation across different timescales.

B. Problem Formulation

Based on the flexible coupler array, we aim to maximize the achievable sum rate of the users by jointly designing the mechanical beamforming matrix $\mathbf{G}(\mathbf{q})$ in the fast timescale and the active-antenna position vector $\mathbf{p}$ in the slow timescale, subject to the radiation-pattern energy constraint and the active-antenna position constraints. To simplify the optimization, we directly optimize the induced mechanical beamforming matrix $\mathbf{G}$ over a predefined radiation-pattern dictionary generated by candidate coupler positions. Thus, the design is formulated as

$$\text{(P1)} \max_{\mathbf{p},\mathbf{G}} \ \mathbb{E}\Big[R(\mathbf{p},\mathbf{G})\Big] \tag{19a}$$

$$\text{s.t.} \ \ \|\mathbf{g}_n\|^2 = 1, \quad \forall n, \tag{19b}$$

$$0 \le p_n \le X, \forall n, \tag{19c}$$

$$|p_n - p_{n'}| \ge d_{\min}, \ \forall n \ne n', \tag{19d}$$

where constraint (19b) normalizes the radiation pattern energy of each antenna to ensure fairness across antenna elements. Constraint (19c) confines active antenna positions within the physical limits of the slide rail. Constraint (19d) enforces a minimum separation between antennas to avoid collisions and excessive mutual coupling. In (19a), $\mathbb{E}[\cdot]$ denotes the expectation over multipath channel realizations at the fast timescale, conditioned on the scattering cluster-core statistics at the slow timescale. To address problem (P1), we need to overcome the following two challenges.

1) *Limited real data in high-dimensional antenna configurations.* Collecting user-level channels for every position-radiation combination of a flexible coupler array is prohibitively time-consuming and costly. A lightweight digital agent is therefore needed to provide reliable statistical CSI and performance surrogates within real-time constraints.
2) *Cross-timescale coupling between active antenna position and mechanical beamforming.* When a conventional two-timescale optimization scheme [28] is used to solve problem (P1), each slow-timescale update triggers a full re-execution of the fast-timescale inner loop, which creates nested outer-inner iterations. The overall complexity thus scales rapidly with the number of antennas, leading to heavy computational load and substantial online latency.

In the following subsections, we present a novel digital-agent-based antenna algorithm that enables intelligent optimization of active antenna position and mechanical beamforming, thereby addressing the two challenges.

IV. Antenna Position and Mechanical Beamforming Design via Digital Agent

In this section, we first describe the design of fast timescale mechanical beamforming, and then elaborate on the construction of the antenna digital agent for slow timescale active-antenna position vector optimization.

A. Fast Timescale Mechanical Beamforming

At the fast timescale, mechanical beamformer $\mathbf{G}$ mainly aims to establish a basic antenna pattern alignment with the statistical multipath channel. In each fast timescale frame, the BS first estimates the statistical multipath channel given active antenna-position vector $\mathbf{p}$, and then obtains the fast timescale mechanical beamforming matrix by solving

$$\text{(P2)} \max_{\mathbf{G}} \ \tilde{R}(\mathbf{G}) \tag{20a}$$

$$\text{s.t.} \ \|\mathbf{g}_n\|^2 = 1, \ \forall n, \tag{20b}$$

where $\tilde{R}(\mathbf{G}) = \mathbb{E}[R(\mathbf{G})] \triangleq \frac{1}{Z_s}\sum_{t=1}^{Z_s} R\big(\mathbf{G};\mathbf{H}^{(t)}\big)$ denotes the ergodic sum-rate evaluated over Z_s fast-timescale channel samples $\mathbf{H}^{(t)} \in \mathbb{C}^{MN\times K}$ given in (17), which are generated based on statistical CSI. The statistical CSI is obtained during uplink channel estimation, where all users simultaneously transmit pilot signals to the BS, and the BS applies the space alternating generalized expectation maximization (SAGE) algorithm to extract the channel statistics [29].

Considering the hardware implementability of mechanically controlled flexible couplers, we adopt a practical approach by selecting the optimal radiation pattern from a predefined set, rather than designing arbitrary patterns with unrestricted directions and shapes. This approach ensures a balance between implementation efficiency and real-world hardware constraints. To be specific, the mechanical beamforming matrix is reformulated as

$$\mathbf{G} = \mathbf{Q}\mathbf{S}, \tag{21}$$

where $\mathbf{Q} = \mathbf{I}_N \otimes \overline{\mathbf{Q}} \in \mathbb{R}^{MN\times UN}$ with $\overline{\mathbf{Q}} \in \mathbb{R}^{M\times U}$ denotes a predefined dictionary that contains the radiation patterns generated under U candidate patterns over M spatial sampling angles. The matrix

$$\mathbf{S} \triangleq \text{blkdiag}\{\mathbf{s}_1, \mathbf{s}_2, \ldots, \mathbf{s}_N\} \in \{0,1\}^{UN\times N}, \tag{22}$$

denotes the radiation-pattern selection matrix, where each $\mathbf{s}_n \in \{0,1\}^U$ is a one-hot vector satisfying $\|\mathbf{s}_n\|_1 = 1$, which selects one candidate state of the coupler-position vector $\mathbf{q}_n$, and thus the corresponding radiation pattern, from the dictionary. By substituting (21) into (18), we have

$$\tilde{R}(\mathbf{S}) = \mathbb{E}\left[\log_2 \det\left(\mathbf{I}_N + \frac{\rho}{\sigma^2}\mathbf{S}^H\mathbf{Q}^H\mathbf{H}(\mathbf{p})\mathbf{H}^H(\mathbf{p})\mathbf{Q}\mathbf{S}\right)\right] \tag{23a}$$

$$= \mathbb{E}\left[\log_2 \det\left(\mathbf{I}_K + \frac{\rho}{\sigma^2}\mathbf{H}^H(\mathbf{p})\mathbf{Q}\mathbf{S}\mathbf{S}^H\mathbf{Q}^H\mathbf{H}(\mathbf{p})\right)\right], \tag{23b}$$

where (23b) is obtained based on Sylvester's determinant theorem, i.e., $\det(\mathbf{I}+\mathbf{A}\mathbf{B}) = \det(\mathbf{I}+\mathbf{B}\mathbf{A})$ [30].

Based on the formulation in (23b), the original problem in (P2) is equivalently transformed into a more practical optimization problem focused on optimizing the radiation pattern-selection matrix $\mathbf{S}$, given by

$$\max_{\mathbf{S}} \ \tilde{R}(\mathbf{S}) \tag{24a}$$

$$\text{s.t.} \ \ [\mathbf{s}_n]_u \in \{0,1\}, \ \forall n, u, \tag{24b}$$

$$\|\mathbf{s}_n\|_1 = 1, \ \forall n. \tag{24c}$$

The non-convex optimization problem in (24) is particularly challenging because the Boolean constraint (24b) is both non-smooth and non-convex. The optimal selection algorithm is an exhaustive search over all possible radiation pattern combinations. However, since the total number of feasible pattern selections is U^N, exhaustive search is impractical due to the extremely large number of possible antenna pattern combinations. Hence, a more tractable optimization strategy is required. Specifically, for each fast-timescale channel sample, we let

$$\mathbf{W}_t = (\mathbf{H}^{(t)}(\mathbf{p}))^H\mathbf{Q} \in \mathbb{C}^{K\times UN}. \tag{25}$$

Moreover, since $\mathbf{S}$ is a block diagonal matrix and each $\mathbf{s}_n$ is a binary indicator vector with exactly one unity entry, the product $\mathbf{S}\mathbf{S}^H$ becomes a diagonal selection matrix. Its diagonal is given by $\mathbf{v} \triangleq [\mathbf{s}_1^T, \ldots, \mathbf{s}_N^T]^T \in \{0,1\}^{UN}$. Therefore, we obtain

$$\text{diag}(\mathbf{v}) = \mathbf{S}\mathbf{S}^H \in \mathbb{C}^{UN\times UN}. \tag{26}$$

By substituting (25) and (26) into (23b), the ergodic sum-rate reduces to

$$\tilde{R}(\mathbf{v}) = \frac{1}{Z_\text{s}}\sum_{t=1}^{Z_\text{s}} \log_2 \det\left(\mathbf{I}_K + \tfrac{\rho}{\sigma^2}\,\mathbf{W}_t\text{diag}(\mathbf{v})\mathbf{W}_t^H\right). \tag{27}$$

We then optimize the binary selector, $\mathbf{v} \in \{0,1\}^{UN}$, to maximize $\tilde{R}(\mathbf{v})$ subject to per-antenna selection constraints. Since the variables in $\mathbf{v}$ are binary integer, the optimization problem becomes NP-hard. To overcome this challenge, we relax the binary constraint on each element of $\mathbf{v}$ to a weaker continuous constraint such that $[\mathbf{v}]_i \in [0,1]$. The original problem in (24) can be relaxed to the following problem.

$$\max_{\mathbf{v}} \ \frac{1}{Z_\text{s}}\sum_{t=1}^{Z_\text{s}} \log_2 \det\left(\mathbf{I}_K + \tfrac{\rho}{\sigma^2}\,\mathbf{W}_t\text{diag}(\mathbf{v})\mathbf{W}_t^H\right) \tag{28a}$$

$$\text{s.t.} \ \ \sum_{u=1}^{U}[\mathbf{v}]_{\phi(n,u)} = 1, \ n = 1,\ldots,N, \tag{28b}$$

$$0 \le [\mathbf{v}]_i \le 1, \ i = 1,\ldots,UN. \tag{28c}$$

where $\phi(n,u) = u + (n-1)U$. Problem (28) is a convex optimization problem that can be solved in polynomial time using CVX [31].

After solving problem (28) and obtaining the optimal relaxed solution $\mathbf{v}^*$, we recover a feasible per-antenna binary selection vector by groupwise rounding. Specifically, for each flexible coupler antenna n, we have

$$\chi_n^* = \arg\max_{u\in\{1,\ldots,U\}} [\mathbf{v}^*]_{\phi(n,u)}, \ n = 1,\ldots,N, \tag{29}$$

$$\mathbf{s}_n = \mathbf{e}_{\chi_n^*} \in \{0,1\}^U, \ n = 1,\ldots,N, \tag{30}$$

where $\mathbf{e}_u$ denotes the u-th canonical basis vector in $\mathbb{R}^U$. With the optimal radiation pattern selection vector $\{\mathbf{s}_n\}$ and known radiation pattern dictionary $\mathbf{Q}$, the mechanical beamformer is constructed as $\mathbf{G} = \mathbf{Q}\mathbf{S}$ in (21).

The computational complexity of solving problem (P2) in each fast timescale mainly depends on the solution of problem (28), whose complexity is of order $\mathcal{O}\Big(\sqrt{2UN}\,\log\left(\frac{1}{\xi}\right)((UN)^3 + Z_\text{s}K^2UN + Z_\text{s}K^3)\Big)$, where ξ denotes the accuracy tolerance of the CVX solver.

B. Digital Agent for Slow Timescale Position Optimization

Over the slow timescale, active-antenna position vector $\mathbf{p}$ is optimized to place the array in the vicinity of the scattering-cluster cores and users, thereby strengthening the large-scale channel links. This design relies only on cluster-core information, namely the estimated nominal distances from users/antennas to the cluster cores. Accordingly, the cluster-core channel, $\mathbf{h}_{\text{C},k}(\mathbf{p})$, is defined as

$$\mathbf{h}_{\text{C},k}(\mathbf{p}) = \bar{\mathbf{Z}}_{\text{C},k}\,\bar{\mathbf{h}}_{\text{C},k}(\mathbf{p}) \in \mathbb{C}^{MN}, \tag{31}$$

where $\bar{\mathbf{h}}_{\text{C},k}(\mathbf{p}) \in \mathbb{C}^{C_kN}$ collects the spatial-domain channel components contributed by the C_k scattering-cluster cores, and $\bar{\mathbf{Z}}_{\text{C},k} \in \{0,1\}^{MN\times C_kN}$ is a binary mapping matrix that encodes the angle information of the scattering cluster cores. Consequently, we substitute the instantaneous multipath

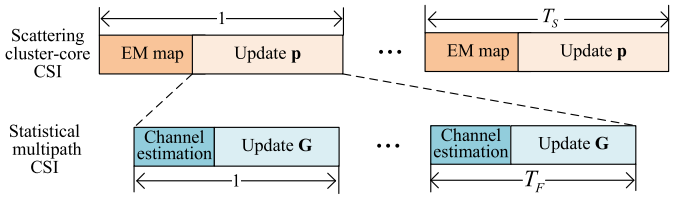

Fig. 4. Proposed slow and fast timescale protocol for flexible coupler array.

channel, $\mathbf{h}_k(\mathbf{p})$, in the channel expression (14b) and the sum-rate formulation (18) with the scattering-cluster-core channel $\mathbf{h}_{\mathrm{C},k}(\mathbf{p})$, thereby defining the slow-timescale sum rate $\tilde{R}(\mathbf{p})$ as our optimization objective. Given mechanical beamformer $\mathbf{G}$, the slow timescale active antenna position design problem is then formulated as

$$\text{(P3)} \ \max_{\mathbf{p}} \ \tilde{R}(\mathbf{p}) \tag{32a}$$

$$\text{s.t.} \ \ 0 \le p_n \le X, \forall n, \tag{32b}$$

$$|p_n - p_{n'}| \ge d_{\min}, \ \forall n \ne n'. \tag{32c}$$

When optimizing the active-antenna position vector in (P3), deriving closed-form expressions of the achievable sum rates of all users, $\tilde{R}(\mathbf{p})$, in terms of the active-antenna position vector $\mathbf{p}$ only is difficult, because we are unable to obtain the optimal mechanical beamforming matrices as explicit functions of the active-antenna position vectors. As the number of antennas and the number of candidate positions increase, nested iterations over the resulting large parameter space under the strict latency requirements of future wireless links become infeasible for conventional control loops. To make the problem tractable, we propose an SFP surrogate training approach with a digital agent, where the surrogate of the objective function is constructed based on appropriately generated channel realizations/samples and the current active-antenna position vector.

An overview of antenna digital agent-based wireless systems is given in Fig. 5. The framework leverages the EM map to generate statistical channel information across different active antenna positions and user locations. Based on this synthetic dataset, a deep neural network is trained to learn an SFP surrogate that captures the coupling between active antenna position and mechanical beamforming. To enhance generalization, the surrogate is further fine-tuned using a limited number of real channel measurements. This digital-agent-assisted algorithm enables efficient position optimization at the slow timescale and mechanical beamforming design at the fast timescale, while avoiding the nested iterations required in conventional two-timescale algorithms. The proposed antenna digital agent comprises the following steps.

1) EM Map: According to (14), besides active-antenna position vector $\mathbf{p}$, the wireless channel is determined by the environmental model, the user position distribution, and the propagation operator, which captures how EM waves interact with the medium and surrounding objects. In an ideal implementation, the agent would maintain up-to-date information on all dynamic scatterers. However, real-time mapping of every movable antenna is often impractical due to cost, power, and computational constraints. Since large-scale propagation parameters are determined by the environmental geometry and user positions, path loss and angular characteristics exhibit slow temporal variation. This makes it feasible to pre-store a set of statistical information within the EM map (also referred to as channel knowledge map [26]). Unlike existing channel knowledge maps [26], which aim to predict instantaneous channel parameters by mapping geographic locations to instantaneous channel realizations, the EM map here stores slowly varying statistical channel information. This approach is to reduce the overhead of channel reconstruction.

Specifically, analogous to the angle index graph constructed in [26], we assume the existence of an ideal EM map that contains the geometry and material data of the environment. The EM map represents the environment by a 3D EM model, denoted by ω, which encodes the positions and EM properties of the BS, user terminals, and static reflectors or scatterers. The 3D EM model, ω, can be reconstructed from sensors or preexisting geographic databases. Consequently, given active antenna position control information, the statistical channel information in the EM map is expressed as

$$\Xi_{k,c,n} = \{\bar{r}_{c,n}, \bar{r}_{k,c}, \varsigma^2_{n,c}, \iota^2_{k,c}\} \tag{33a}$$

$$= \mathrm{EMM}\big(\omega, \upsilon_k, p_n\big), \tag{33b}$$

for arbitrary active antenna positions p_n, scatterers c, and user locations υ_k, where $\mathrm{EMM}(\cdot)$ denotes the location-to-statistical-channel mapping function. The constructed EM map essentially serves as a database rooted in the location domain and establishes a mapping between user locations, antenna parameters, and statistical channel information, thereby guiding both active antenna position optimization and mechanical beamforming design.

2) Label Data Generation With Optimized Mechanical Beamforming: We generate multiple samples of active antenna positions. $\{\mathbf{p}_j\}_{j=1}^{N_\mathrm{s}}$ such that the active antenna position space is uniformly covered, where the subscript j is used to denote the index of the j-th training sample, and N_s is the total number of samples. Based on the EM map, we then generate the cluster-core channel $\tilde{\mathbf{H}}_C(\mathbf{p}_j) \in \mathbb{C}^{MN\times K}$ for every active-antenna position vector $\mathbf{p}_j$. Moreover, for every $\mathbf{p}_j$, we draw Z_s statistical multipath channel realizations, denoted by $\{\tilde{\mathbf{H}}_{j,i}(\mathbf{p}_j)\}_{i=1}^{Z_\mathrm{s}}$ with $\tilde{\mathbf{H}}_{j,i}(\mathbf{p}_j) \in \mathbb{C}^{MN\times K}$, conditioned on cluster core and multipath statistics obtained in EM map. Specifically, for each cluster c, we draw per-realization sub-rays $\{r_{l_c,n}, r_{k,c,l_c}\}$ around $\{\bar{r}_{c,n}, \bar{r}_{k,c}\}$ according to $\{\varsigma^2_{n,c}, \iota^2_{k,c}\}$.

The resulting channel matrix samples can then be post-processed to extract key performance indicators. Specifically, given the set $\{\tilde{\mathbf{H}}_{j,i}(\mathbf{p}_j)\}_{i=1}^{Z_\mathrm{s}}$, we solve the fast-timescale ray-level problem (P2) to obtain the corresponding set of optimized matrices $\{\mathbf{G}_j^*\}$.

Next, by substituting the obtained $\mathbf{G}_j^*$, $\mathbf{p}_j$, and the cluster-core channel $\tilde{\mathbf{h}}_{\mathrm{C},k}(\mathbf{p}_j)$ into the objective function of problem (P3), we obtain the sum rate of all users for active antenna position $\mathbf{p}_j$ as $\bar{R}_j$. Then, the tuple $\big(\tilde{\mathbf{H}}_j(\mathbf{p}_j), \bar{R}_j\big)$ is referred to as the j-th training sample, where $\tilde{\mathbf{H}}_j(\mathbf{p}_j) = \left\{\left\{\tilde{\mathbf{H}}_{j,i}\left(\mathbf{p}_j\right)\right\}_{i=1}^{Z_\mathrm{s}}, \tilde{\mathbf{H}}_C\left(\mathbf{p}_j\right)\right\}$. We repeat the above process multiple times to generate the entire training data set.

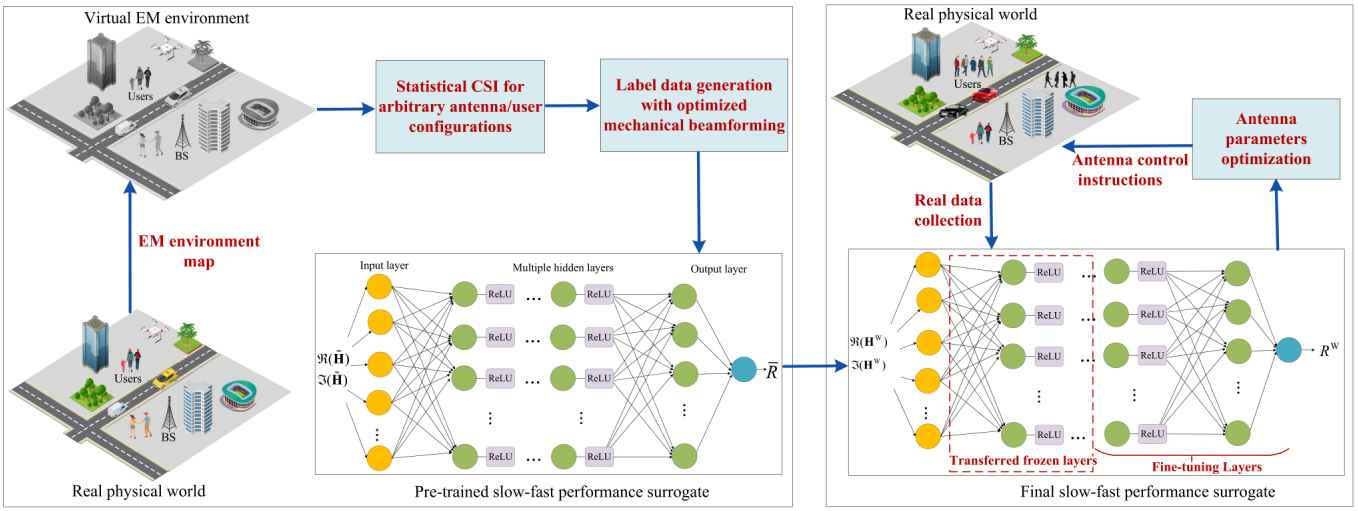

(a) Antenna digital agent pre-training (b) Antenna digital agent online fine-tuning and control

Fig. 5. The proposed antenna digital agent architecture.

3) Slow-Fast Performance Surrogate Pre-Training: The SFP surrogate is a data-driven function that takes statistical cluster-core and multipath channel as input and directly predicts the corresponding optimized user sum rate, which already accounts for the fast-timescale mechanical-beamforming optimization. In the following, the elements of the chosen deep neural network model for SFP surrogate training are described.

The proposed deep neural network architecture is designed as a Multi-Layer Perceptron network, which is well-established as a universal function approximator [32]. The proposed network consists of $\bar{Q}$ layers, as illustrated in Fig. 5. The network alternates between fully connected and nonlinear layers. The q-th layer in the network has a stack of N_q neurons. For the non-linearity layers, Rectified Linear Units (ReLUs) are employed [33]. The input of the network is the real and imaginary parts of channel $\tilde{\mathbf{H}}$, and the output of the network is the sum rate $\bar{R}$. This model learns how to map an input (i.e., sampled channel vector) to an output (i.e., predicted achievable rate). All samples are normalized using dataset-level scaling [33], i.e., $\tilde{\mathbf{H}}^{\text{norm}} = \frac{\tilde{\mathbf{H}}}{\Delta}$ with $\Delta = \max_{i,j}|[\tilde{\mathbf{H}}]_{i,j}|$. This normalization choice preserves distance information encoded in the environment descriptors. Since modern implementations of deep learning models mainly use real-valued computations, each complex entry of the input data is split into real and imaginary values. For output normalization, let $R_{\max} = \max_{j\in\mathcal{J}} \bar{R}_j$ be the largest sum-rate value in the training set, where $\mathcal{J} = \{1, 2, \cdots, N_{\text{s}}\}$. Prior to training, each label is normalized as $\frac{\bar{R}_j}{R_{\max}}, \forall j \in \{1, 2, \cdots, N_{\text{s}}\}$.

Let $F_{\boldsymbol{\tau}}(\tilde{\mathbf{H}}(\mathbf{p})) : \mathbb{R}^{MN} \to \mathbb{R}$ denote the proposed neural network with parameters $\boldsymbol{\tau}$. We use the entire training data set, $\{\tilde{\mathbf{H}}_j(\mathbf{p}_j), \bar{R}_j\}$, to optimize the weights of the neural network $\boldsymbol{\tau}$. The cost function is defined as the mean squared error (MSE) between the label $\bar{R}_j$ and the neural network output. Specifically, the model is trained using a regression loss function. The training is guided through minimizing the following loss function

$$F_{\boldsymbol{\tau}} = \frac{1}{N_{\text{s}}} \sum_{j=1}^{N_{\text{s}}} \left(F_{\boldsymbol{\tau}}(\tilde{\mathbf{H}}_j(\mathbf{p}_j)) - \bar{R}_j\right)^2. \tag{34}$$

After convergence, surrogate $F_{\boldsymbol{\tau}}$ accurately predicts the expected sum-rate that is already maximized over $\mathbf{G}$, rendering the inner mechanical beamforming optimization loop unnecessary online.

4) Fine-Tuning for Accurate Position Optimization: Wireless networks exhibit inherent dynamics in both large-scale and small-scale statistics. In our two-timescale framework, cluster-core statistics vary slowly, whereas intra-cluster multipath-ray statistics fluctuate rapidly and are already handled by the fast-timescale mechanical-beamforming optimizer for $\mathbf{G}$ in problem (P2). Consequently, the offline-learned SFP surrogate may become mismatched at the slow timescale, leading to performance degradation when applied online. To mitigate this issue, we adopt a transfer-learning strategy [34], where the online deep neural network (DNN) is initialized by the offline SFP model and subsequently fine-tuned using a limited number of newly labeled samples from the current environment.

Specifically, we collect a small set of samples that capture the present channel conditions:

$$\left\{\mathbf{H}_j^{\text{W}}(\mathbf{p}_j),\, \bar{R}_j^{\text{W}}\right\}_{j=1}^{N_{\text{w}}}, \qquad N_{\text{w}} \ll N_{\text{s}}, \tag{35}$$

where $\mathbf{H}_j^{\text{W}}(\mathbf{p}_j)$ denotes the collected channel samples for active antenna position $\mathbf{p}_j$, $\bar{R}_j^{\text{W}}$ is the corresponding average sum rate, and N_{w} is the number of newly collected channel samples for fine-tuning, which is much smaller than the size of the offline training dataset N_{s}.

Then, we refine the pre-trained SFP network via domain adaptation, where a subset of layers is frozen, and only the remaining layers are fine-tuned so that the DNN adapts to the current cluster-core channel coefficients. Mathematically,

$$F_{\bar{\boldsymbol{\tau}}}(\mathbf{H}^{\text{W}}(\mathbf{p})) = F_{\bar{\boldsymbol{\tau}}}^{\text{FL}}\left(F_{\boldsymbol{\tau}^*}^{\text{TL}}(\mathbf{H}^{\text{W}}(\mathbf{p}))\right), \tag{36}$$

TABLE I
SIMULATION PARAMETERS

Parameter	Description	Value
η	Learning rate for training the DNN	0.01
S_B	Number of training iterations for pre-training	1000
S_T	Number of training iterations for fine tuning	100
B	Batch size for split training and testing sets	32
ϵ	Smoothing term to prevent division by zero for Adam	10^{-8}
N_{s}	Number of training samples used for pre-training	10^5
N_{W}	Number of training samples used for retraining in a mismatch scenario	10^3

where $F^{\mathrm{TL}}_{\boldsymbol{\tau}^*}(\cdot)$ denotes the frozen layers with parameters $\boldsymbol{\tau}^*$ obtained in the pre-training stage, and $F^{\mathrm{FL}}_{\bar{\boldsymbol{\tau}}}(\cdot)$ denotes the fine-tuned layers with updated parameters $\bar{\boldsymbol{\tau}}$. Because only the small set $\{\mathbf{H}^{\mathrm{W}}_j(\mathbf{p}_j), R^{\mathrm{W}}_j\}$ is required, the online retraining time meets the stringent latency requirements of the flexible coupler system.

Replacing the objective function in problem (P3) by the learned SFP surrogate yields

$$(\mathrm{P4}) \max_{\mathbf{p}} \; F_{\bar{\boldsymbol{\tau}}}\big(\mathbf{H}^{\mathrm{W}}(\mathbf{p})\big) \tag{37a}$$

$$\text{s.t. } 0 \le p_n \le X, \; \forall n, \tag{37b}$$

$$|p_n - p_{n'}| \ge d_{\min}, \; \forall n \ne n'. \tag{37c}$$

where $F_{\bar{\boldsymbol{\tau}}}(\cdot)$ is a trained neural surrogate evaluated numerically. Based on problem (P4), the BS observes the current cluster-core CSI feature and updates $\mathbf{p}$ via projected gradient ascent [35]. By indexing the flexible coupler antennas along the rail in nondecreasing order of their positions (i.e., $p_1 \le \cdots \le p_N$), the nonconvex constraints (37c) can be simplified as the following linear constraints:

$$p_n - p_{n-1} \ge d_{\min}, \forall n = 2, \cdots, N. \tag{38}$$

Then, we define

$$\mathcal{T} \triangleq \Big\{ \mathbf{p} \in \mathbb{R}^N : 0 \le p_1, \; p_{n+1} - p_n \ge d_{\min} \; (n = 1, \; \ldots, N-1), \; p_N \le X \Big\}, \tag{39}$$

as a nonempty and closed convex polyhedron. Note that $\mathcal{T}$ is guaranteed to be nonempty since $X \ge (N-1)d_{\min}$. Next, for iteration t, we execute

$$\mathbf{e}^{(t)} = \nabla_{\mathbf{p}} F_{\bar{\boldsymbol{\tau}}}\big(\mathbf{H}^{\mathrm{W}}(\mathbf{p}^{(t)})\big), \tag{40a}$$

$$\mathbf{p}^{(t+1)} = \mathrm{Proj}_{\mathcal{T}}\big(\mathbf{p}^{(t)} + \eta\, \mathbf{e}^{(t)}\big), \tag{40b}$$

and terminate when $\|\mathbf{e}^{(t)}\| < \varepsilon$, where ε is a predefined tolerance and η is the fixed step size of the projected-gradient update [36]. Here, the Euclidean projection $\mathrm{Proj}_{\mathcal{T}}(\mathbf{x})$ maps any vector $\mathbf{x}$ onto the closed convex set $\mathcal{T}$ by returning the unique point in $\mathcal{T}$ that minimizes the Euclidean distance to $\mathbf{x}$.

The overall digital agent-assisted two-timescale optimization algorithm for flexible coupler array is detailed in Algorithm 1. The algorithm guarantees convergence to local optimal points since the objective value is non-decreasing in each iteration. In Algorithm 1, the computational complexity of active antenna position optimization is $\mathcal{O}(2K + 2LMN^3 + 2KLN)$ where $L = \max\{L_1, L_2, \ldots, L_K\}$ [34].

V. SIMULATION RESULTS

In the simulation, the users are randomly distributed within a two-dimensional rectangular region of size $S_x = 8$ m by $S_y = 15$ m. The total number of flexible coupler antennas is $N = 16$. The carrier frequency is 28 GHz. We set $U = 14$ and $M = 360$. In this scenario, all $K = 10$ users operate under a scattering-cluster channel with $C_k = 3$ clusters, each consisting of $L_{c,k} = 3$ multipaths. The nominal distances of these scattering clusters, $\bar{r}_{c,n}$ and $\bar{r}_{k,c}$, are randomly drawn from the range $[2, 4]$ m, while the distance spreads are set to $\varsigma_{n,c} = 0.4$ m and $\iota_{k,c} = 0.4$ m. In the proposed digital agent algorithm, the DNN is composed of four dense layers, with the number of neurons as 500, 250, 100, and 50, respectively. Unless otherwise specified, the simulation parameters are summarized in Table I. The EM map is constructed via intelligent ray tracing [37], where physical paths are grouped in the joint angle and delay domain. For each cluster, we compute the mean delay and the delay variance. These statistics determine the cluster core distances and the corresponding distance variance parameters for each user and active antenna position.

We consider the traditional two-timescale optimization structure as the baseline scheme. At the fast timescale, the BS first estimates the statistical CSI and generates multipath channel samples to evaluate the ergodic sum rate, and then obtains the mechanical beamforming matrix by solving problem (P2). At the slow timescale, the BS first computes the cluster-core CSI and then iteratively updates the active-antenna position vector $\mathbf{p}^{(t)}$ using the conditional gradient algorithm [10]. At each outer iteration of the position update, it calls the fast mechanical beamforming subproblem (P2) as the inner loop to obtain $\mathbf{G}^{(t)}$, and the process continues until $\mathbf{p}^{(t)}$ converges. The complexity of updating the slow-timescale position vector $\mathbf{p}$ is $\mathcal{O}\left(I\left(T_{\mathrm{H}} J\left(\sqrt{2UN}\log\frac{1}{\xi}((UN)^3 + Z_{\mathrm{s}}K^2UN + Z_{\mathrm{s}}K^3)\right) + NK^2\right)\right)$ [10], where I denotes the number of iterations in the position optimization, J denotes the number of iterations in the mechanical beamforming, and T_H denotes the number of fast channel samples used per slow-timescale position update.

Fig. 6 compares the proposed digital-agent algorithm with the traditional two-timescale optimization for flexible coupler systems under a deliberately mismatched cluster-core distribution. In this scenario, the nominal distance range of the scattering clusters for each user is enlarged to $[3, 5]$ m, while $\{C_k\}$ and $\{L_{c,k}\}$ remain unchanged. The traditional baseline fails to adapt to channel variations, which results in a sharp decline in the average sum rate. In contrast, the digital agent adapts well to channel information and simultaneously reduces the online complexity of the traditional two-timescale methods to $\mathcal{O}(2K + 2LMN^3 + 2KLN)$. For example, the proposed

Algorithm 1 Digital Agent-Assisted Two-Timescale Optimization Algorithm for Flexible Coupler Array

Inputs: Number of samples N_{s}; step size η; tolerance ε.
Outputs: Active antenna position vector $\mathbf{p}^*$ and mechanical beamformer $\mathbf{G}^*$.
Step 1: Slow timescale active antenna position optimization
- **Antenna digital agent pre-training**
  1) EM map construction.
  2) Generate optimized mechanical beamforming matrices $\{\mathbf{G}_j^*\}$ by running **Step 2** and generate label data.
  3) Calculate the average sum rate $\bar{R}_j$ for $\mathbf{p}_j$.
  4) Repeat the above process multiple times to generate the entire training data set $\{\tilde{\mathbf{H}}_j(\mathbf{p}_j), \bar{R}_j\}_{j=1}^{\tilde{N}_{\mathrm{s}}}$.
  5) A neural network $F_{\boldsymbol{\tau}}(\tilde{\mathbf{H}}(\mathbf{p}))$ is trained by minimizing (34) to serve as a surrogate for SFP.
- **Antenna digital agent online fine-tuning and control**:
  1) Refresh statistical channel state information with the current environment.
  2) Collect retraining data from (35).
  3) Update the fine-tuned DNN parameters $\bar{\boldsymbol{\tau}}$ via (36).
  4) **while** $\|\mathbf{e}^{(t)}\| > \varepsilon$ **do**
  Update $\mathbf{e}^{(t)}$ and $\mathbf{p}^{(t+1)}$ via (40a) and (40b), respectively.
  5) **end while**
  6) Set $\mathbf{p}^* = \mathbf{p}^{(t+1)}$.
Step 2: Fast timescale mechanical beamforming with given $\mathbf{p}^*$
- **while** no convergence of **S do**
  1) Update $\mathbf{v}$ by solving problem (28).
  2) Update radiation pattern selection vector $\mathbf{s}_n$ by (30).
- **end while**
- Construct the mechanical beamformer $\mathbf{G}^*$ by (21).

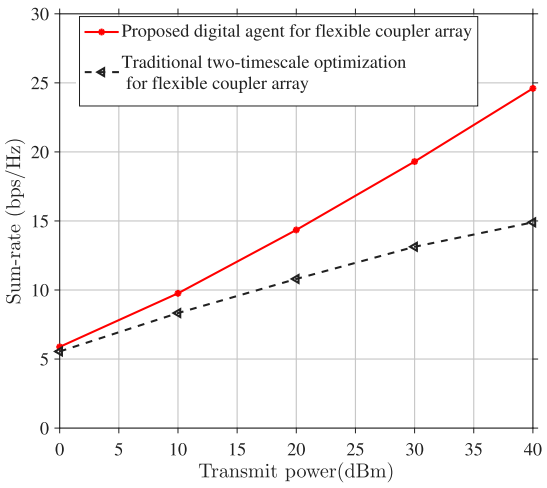

Fig. 6. Comparison of the digital agent and traditional two-timescale optimization algorithms.

digital agent algorithm achieves 95% of the final average sum rate within approximately 32.4 s, whereas the baseline requires approximately 10.9 min, since each slow-timescale update requires rerunning the inner fast-timescale loop. When the channel statistics drift, the agent fine-tunes only the last two network layers with a small number of labeled channel realizations, which preserves adaptability without incurring large online cost. These results indicate that the proposed digital agent ensures reliable performance by solving the optimization within the digital agent rather than relying entirely on the physical environment.

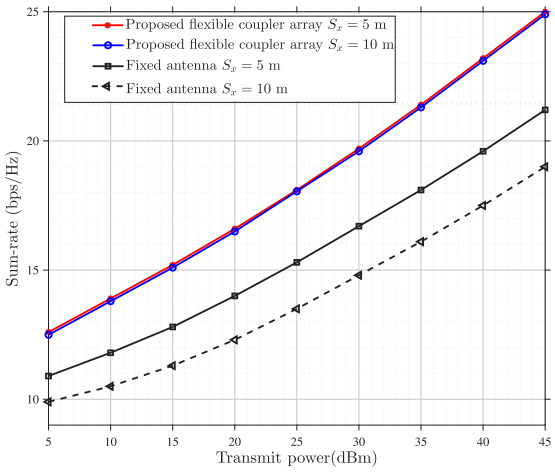

Fig. 7. Impact of the reserved area's horizontal length S_x on flexible coupler system performance.

Fig. 7 illustrates the average sum rate as a function of transmit power for the proposed flexible coupler array and the conventional fixed antenna with fixed position, rotation, and radiation pattern, evaluated for deployment areas with horizontal lengths of $S_x = 5$ m and $S_x = 10$ m. As observed, the proposed flexible coupler array consistently achieves a higher average rate compared to the conventional system, which demonstrates its ability to provide enhanced communication performance. In addition, the average rate of the proposed flexible coupler array remains nearly identical for both deployment areas, while the conventional system experiences a significant degradation when transitioning from $S_x = 5$ m to $S_x = 10$ m. This advantage is attributed to the flexibility of the flexible coupler antenna to adjust its position along the slide rail to be closer to the user, effectively mitigating path loss and maintaining strong communication links. This behavior highlights that the flexible coupler performance is less sensitive to variations in deployment area, which confirms that dynamic positioning effectively mitigates the adverse effects of increased propagation distance. In contrast, the conventional system suffers significant performance degradation due to the fixed position of its antenna, which amplifies the path loss in wireless propagation as the horizontal length S_x increases.

Fig. 8 plots the average sum-rate versus transmit power for the proposed flexible coupler system and fixed-pattern translatable antenna system (i.e., an antenna with a fixed rotation and pattern that can only slide along a rail), evaluated for deployment areas of vertical length $S_y = 8$ m and $S_y = 15$ m.

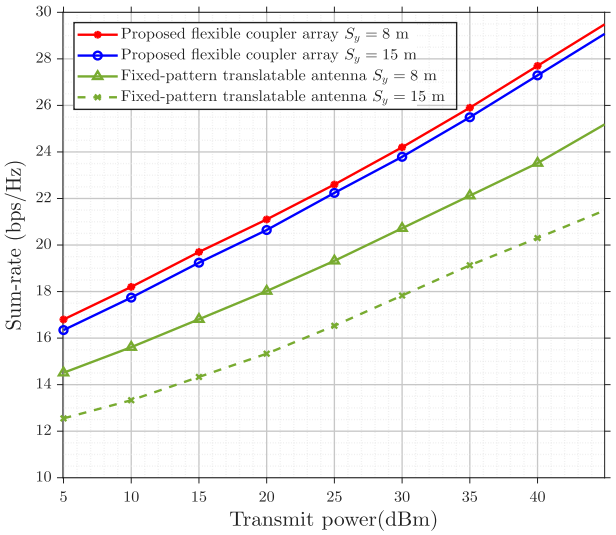

Fig. 8. Impact of the reserved area's vertical length S_y on flexible coupler system performance.

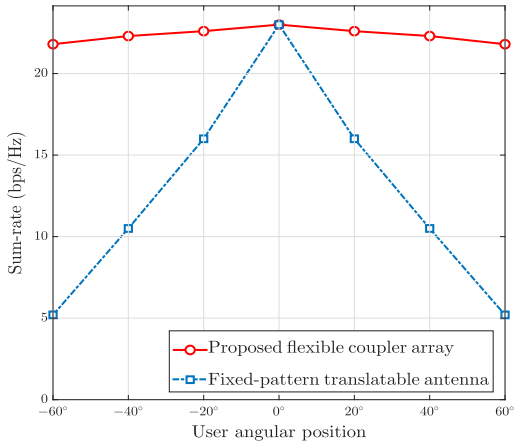

Fig. 9. The sum-rate of flexible coupler system versus the angle of the user.

It can be observed that extending the reserved area increases the propagation distance, thereby degrading the throughput of the fixed-pattern translatable antenna. In contrast, the two curves corresponding to the proposed flexible coupler array remain close, with only minor differences attributable to the additional path loss introduced by the taller service region. These results verify that the combination of sliding mobility and radiation pattern reconfiguration of couplers effectively mitigates the geometric penalty of a larger vertical coverage area, thereby sustaining nearly optimal performance across the entire coverage range. It is worth noting that the robustness of the proposed flexible coupler array is achieved using a single slide rail, as each antenna element can both slide and reshape its radiation pattern. In comparison, the fixed-pattern translatable antenna design typically requires multiple parallel rails to achieve comparable rates, which substantially increases hardware complexity and deployment cost.

Fig. 9 illustrates the sum-rate variation with respect to the user's angular position relative to the flexible coupler array, where $K = 1$ and $N = 1$. The proposed flexible coupler array maintains robust performance across a wide range of user angles by dynamically adjusting the pattern orientations as the user position deviates from the optimal direction.

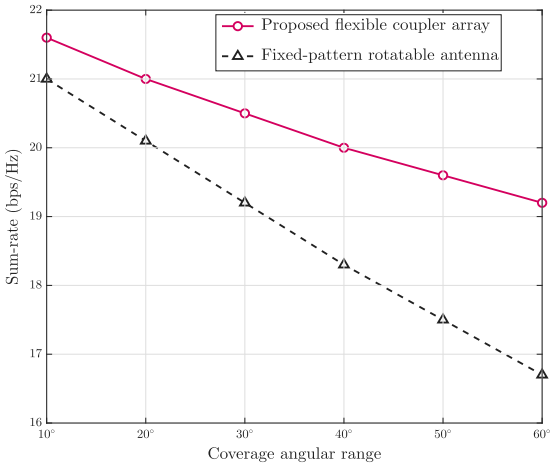

Fig. 10. The sum-rate of flexible coupler system versus the coverage angular range.

In contrast, the fixed-pattern translatable antenna achieves satisfactory performance only when the user is positioned perpendicularly to the array, where the antenna gain is maximized. These results underscore the robustness and versatility of the proposed mechanical beamforming approach, demonstrating that dynamic pattern reconfiguration not only compensates for variations in user location but also substantially enhances the overall system performance and reliability across diverse deployment scenarios.

Fig. 10 presents the average sum rate versus the total user coverage angle for two antenna configurations, namely proposed flexible coupler array with fixed active antenna positions and the rotatable antenna with a fixed radiation pattern (i.e., the active antenna remains at a fixed position with a fixed pattern, but it can rotate around its own axis). We can see that when the coverage angular range is small, both schemes achieve similar performance because their main lobes can remain aligned with the users. As the angle increases (i.e., the users are more widely dispersed), the fixed-pattern rotatable antenna experiences rapid performance degradation due to misalignment. By contrast, the proposed flexible coupler array exhibits a much slower performance decline, since coupler movement keeps the array oriented toward the prevailing user sector, while pattern reconfiguration compensates for residual offsets and angular dispersion among users. These results indicate that flexible coupler array is essential for sustaining high sum-rate performance over wide angular coverage.

VI. Conclusion

We have proposed a flexible coupler antenna array that combines the small-range relocation of passive couplers with large-scale antenna translation. The array introduces an additional radiation DoF with relocating couplers and reduces large-scale path loss by enabling near-user placement. We have then designed a two-timescale optimization framework that maximizes the sum rate by jointly optimizing active antenna position at the slow timescale and mechanical beamforming at the fast timescale. To solve this problem, we have proposed a digital-agent-aided optimization algorithm to reduce online computational complexity. The proposed coupler position reconfiguration provides a cost-effective way to enhance

communication performance without moving active antennas, thereby improving antenna adaptability with a compact structure and low hardware overhead. For our future work, we will investigate channel estimation for the flexible coupler array, since each new configuration of passive coupler positions results in a different channel as well as varied coupling with the active antenna element.

REFERENCES

[1] E. G. Larsson, O. Edfors, F. Tufvesson, and T. L. Marzetta, "Massive MIMO for next generation wireless systems," *IEEE Commun. Mag.*, vol. 52, no. 2, pp. 186–195, Feb. 2014.

[2] C. Qi, K. Chen, O. A. Dobre, and G. Y. Li, "Hierarchical codebook-based multiuser beam training for millimeter wave massive MIMO," *IEEE Trans. Wireless Commun.*, vol. 19, no. 12, pp. 8142–8152, Dec. 2020.

[3] B. Di, H. Zhang, Z. Han, R. Zhang, and L. Song, "Reconfigurable holographic surface: A new paradigm for ultra-massive MIMO," *IEEE Trans. Cognit. Commun. Netw.*, vol. 11, no. 6, pp. 3761–3783, Dec. 2025.

[4] B. Di, Y. Zhang, R. Deng, M. Wang, S. Sun, and L. Song, "Holographic metasurfaces for extremely large-scale MIMO communications: Design, implementation, and experiment results," *IEEE Wireless Commun.*, early access, Nov.14, 2025, doi: 10.1109/MWC.2025.3625029.

[5] X. Yue et al., "Federated learning in active STARS-aided uplink networks," *IEEE Trans. Veh. Technol.*, vol. 75, no. 1, pp. 1156–1170, Jan. 2026.

[6] X. Yue, J. Xie, C. Ouyang, Y. Liu, X. Shen, and Z. Ding, "Active simultaneously transmitting and reflecting surface assisted NOMA networks," *IEEE Trans. Wireless Commun.*, vol. 23, no. 8, pp. 9912–9926, Aug. 2024.

[7] Q. Wu et al., "Intelligent surfaces empowered wireless network: Recent advances and the road to 6G," *Proc. IEEE*, vol. 112, no. 7, pp. 724–763, Jul. 2024.

[8] R. Li, S. Sun, and M. Tao, "Atomic norm minimization-based DoA estimation for IRS-assisted sensing systems," *IEEE Wireless Commun. Lett.*, vol. 13, no. 10, pp. 2672–2676, Oct. 2024.

[9] Y. Li, C. Qi, S. Mao, and O. A. Dobre, "Tri-hybrid beamforming for radiation-center reconfigurable antenna array: Spectral efficiency and energy efficiency," *IEEE Trans. Wireless Commun.*, vol. 25, pp. 12263–12278, 2026.

[10] X. Shao, Q. Jiang, and R. Zhang, "6D movable antenna based on user distribution: Modeling and optimization," *IEEE Trans. Wireless Commun.*, vol. 24, no. 1, pp. 355–370, Jan. 2025.

[11] X. Shao, R. Zhang, Q. Jiang, and R. Schober, "6D movable antenna enhanced wireless network via discrete position and rotation optimization," *IEEE J. Sel. Areas Commun.*, vol. 43, no. 3, pp. 674–687, Mar. 2025.

[12] X. Shao and R. Zhang, "6DMA enhanced wireless network with flexible antenna position and rotation: Opportunities and challenges," *IEEE Commun. Mag.*, vol. 63, no. 4, pp. 121–128, Apr. 2025.

[13] Z. Wang, Y. Zhao, G. Hu, Y. Zheng, and K. Yang, "6D movable holographic surface assisted integrated data and energy transfer: A sensing enhanced approach," 2025, *arXiv:2510.21137*.

[14] X. Shao, R. Zhang, Q. Jiang, J. Park, T. Q. S. Quek, and R. Schober, "Distributed channel estimation and optimization for 6D movable antenna: Unveiling directional sparsity," *IEEE J. Sel. Topics Signal Process.*, vol. 19, no. 2, pp. 349–365, Mar. 2025.

[15] W. Yan, W. Hao, Y. Fan, Y. Guo, Q. Wu, and X. Li, "Six-dimensional movable antenna enabled wideband THz communications," 2025, *arXiv:2510.25088*.

[16] C. Liu, W. Mei, P. Wang, Y. Meng, B. Ning, and Z. Chen, "UAV-enabled passive 6D movable antennas: Joint deployment and beamforming optimization," 2024, *arXiv:2412.11150*.

[17] X. Shao et al., "A tutorial on six-dimensional movable antenna for 6G networks: Synergizing positionable and rotatable antennas," *IEEE Commun. Surveys Tuts.*, vol. 28, pp. 3666–3709, 2026.

[18] P. Wang, Y. Xue, W. Mei, J. Fang, and R. Zhang, "UAV-enabled passive 6D movable antenna for ISAC: Joint location, orientation, and reflection optimization," *IEEE Wireless Commun. Lett.*, vol. 14, no. 12, pp. 3982–3986, Dec. 2025.

[19] X. Shao et al., "Polarforming antenna enhanced sensing and communication: Modeling and optimization," *IEEE J. Sel. Areas Commun.*, vol. 44, pp. 416–431, 2026.

[20] K.-K. Wong, A. Shojaeifard, K.-F. Tong, and Y. Zhang, "Fluid antenna systems," *IEEE Trans. Wireless Commun.*, vol. 20, no. 3, pp. 1950–1962, Mar. 2021.

[21] X. Shao, C. Shan, W. Zhuang, and X. Shen, "Coupler position optimization and channel estimation for flexible coupler antenna aided multiuser communication," 2026, *arXiv:2602.11319*.

[22] X. Shao, C. Shan, W. Zhuang, and X. Shen, "Flexible coupler antenna for wireless networks: Opportunities and challenges," *IEEE Commun. Mag.*, 2026.

[23] J. Zheng, T. H. Luan, Y. Zhang, G. Li, Z. Su, and W. Wu, "Digital twin in 6G: Embracing comprehensive network intelligence," *IEEE Wireless Commun.*, vol. 31, no. 6, pp. 94–101, Dec. 2024.

[24] N. Cheng, X. Wang, Z. Li, Z. Yin, T. H. Luan, and X. Shen, "Toward enhanced reinforcement learning-based resource management via digital twin: Opportunities, applications, and challenges," *IEEE Netw.*, vol. 39, no. 1, pp. 189–196, Jan. 2025.

[25] V. B. P. RajratnaKharat, "*Digital twin: Manufacturing excellence through virtual factory replication*," Bureau Municipal Res., Toronto, ON, Canada, White Paper 1,2014, pp. 1–7.

[26] N. Cheng et al., "Channel knowledge map-enabled 6D movable antenna systems with kinematic constraints: A manifold optimization approach," *IEEE Trans. Wireless Commun.*, vol. 25, pp. 8968–8981, 2025.

[27] X. Li, J. Fang, H. Li, and P. Wang, "Millimeter wave channel estimation via exploiting joint sparse and low-rank structures," *IEEE Trans. Wireless Commun.*, vol. 17, no. 2, pp. 1123–1133, Feb. 2018.

[28] M.-M. Zhao, Q. Wu, M.-J. Zhao, and R. Zhang, "Intelligent reflecting surface enhanced wireless networks: Two-timescale beamforming optimization," *IEEE Trans. Wireless Commun.*, vol. 20, no. 1, pp. 2–17, Jan. 2021.

[29] B. H. Fleury, M. Tschudin, R. Heddergott, D. Dahlhaus, and K. Ingeman Pedersen, "Channel parameter estimation in mobile radio environments using the SAGE algorithm," *IEEE J. Sel. Areas Commun.*, vol. 17, no. 3, pp. 434–450, Mar. 1999.

[30] A. G. Akritas, E. K. Akritas, and G. I. Malaschonok, "Various proofs of Sylvester's (determinant) identity," *Math. Comput. Simul.*, vol. 42, nos. 4–6, pp. 585–593, Nov. 1996.

[31] D. Bertsekas, *Convex Optimization Algorithms*. Belmont, MA, USA: Athena Scientific, 2015.

[32] K. Hornik, M. Stinchcombe, and H. White, "Multilayer feedforward networks are universal approximators," *Neural Netw.*, vol. 2, no. 5, pp. 359–366, Jan. 1989.

[33] I. Goodfellow, Y. Bengio, A. Courville, and Y. Bengio, *Deep Learning*, vol. 1. Cambridge, MA, USA: MIT Press, 2016.

[34] S. Khan, S. Durrani, and X. Zhou, "Transfer learning based detection for intelligent reflecting surface aided communications," in *Proc. IEEE 32nd Annu. Int. Symp. Pers., Indoor Mobile Radio Commun. (PIMRC)*, Sep. 2021, pp. 555–560.

[35] H. Hassani, M. Soltanolkotabi, and A. Karbasi, "Gradient methods for submodular maximization," in *Proc. Adv. Neural Inf. Process. Syst.*, 2017, pp. 1–11.

[36] J.-C. Chen and Y.-C. Lin, "A projected gradient descent algorithm for designing low-resolution finite-alphabet equalizers in all-digital massive MU-MIMO communication systems," *IEEE Access*, vol. 11, pp. 50744–50751, 2023.

[37] T. Rautiainen, G. Wolfle, and R. Hoppe, "Verifying path loss and delay spread predictions of a 3D ray tracing propagation model in urban environment," in *Proc. IEEE 56th Veh. Technol. Conf.*, vol. 4, Sep. 2002, pp. 2470–2474.

Xiaodan Shao (Member, IEEE) received the Ph.D. degree in information and communication engineering from Zhejiang University, China. She was a Humboldt Research Fellow with the Institute for Digital Communications, Friedrich-Alexander University of Erlangen-Nuremberg (FAU), Erlangen, Germany. She is currently a Post-Doctoral Fellow with the Department of Electrical and Computer Engineering, University of Waterloo, Canada. Her current research interests include six-dimensional movable antenna (6DMA), flexible coupler antenna (FCA), MIMO, statistical signal processing, and machine learning for wireless communication. She was a recipient of the IEEE WCSP Best Paper Award in 2020, the Best Ph.D. Thesis Award of China Institute of Communications in 2023, the IEEE Communications Society Leonard G. Abraham Prize in 2025, the IEEE GLOBECOM Best Paper Award in 2025, and the IEEE VTC Best Paper Award in 2025. She serves as an Associate Editor for IEEE WIRELESS COMMUNICATIONS LETTERSand IEEE TRANSACTIONS ON COMMUNICATIONS.

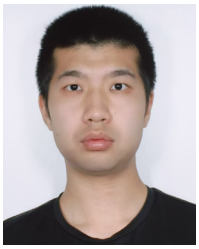

Yixiao Zhang (Graduate Student Member, IEEE) received the B.Eng. degree in communication engineering from Harbin Institute of Technology (HIT), Shenzhen, China, in 2020, and the M.S. degree in machine learning from the KTH Royal Institute of Technology, Stockholm, Sweden, in 2023. He is currently pursuing Ph.D. degree with the Department of Electrical and Computer Engineering, University of Waterloo, Waterloo, ON, Canada. His research interests include network resource management, digital twin, and collaborative robot navigation and control.

Nan Cheng (Senior Member, IEEE) received the B.E. and M.S. degrees from the Department of Electronics and Information Engineering, Tongji University, Shanghai, China, in 2009 and 2012, respectively, and the Ph.D. degree from the Department of Electrical and Computer Engineering, University of Waterloo, Waterloo, ON, Canada, in 2016. From 2017 to 2019, he was a Post-Doctoral Fellow with the Department of Electrical and Computer Engineering, University of Toronto, Toronto, ON, Canada. He is currently a Professor with the State Key Laboratory of ISN and the School of Telecommunications Engineering, Xidian University, Xi'an, Shaanxi, China. He has authored or co-authored more than 90 journal articles in IEEE TRANSACTIONS and other top journals. His research interests include B5G/6G, AI-driven future networks, and space-air-ground-integrated networks. He is an Associate Editor of IEEE TRANSACTIONS ON VEHICULAR TECHNOLOGY, IEEE OPEN JOURNAL OF THE COMMUNICATIONS SOCIETY, and *Peer-to-Peer Networking and Applications*. He is/was a guest editor of several journals.

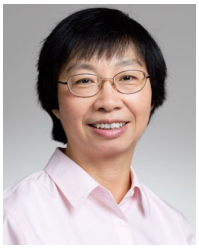

Weihua Zhuang (Fellow, IEEE) received the B.Sc. and M.Sc. degrees in electrical engineering from Dalian Maritime University, China, and the Ph.D. degree in electrical engineering from the University of New Brunswick, Canada. Since 1993, she has been a Faculty Member of the Department of Electrical and Computer Engineering, University of Waterloo, Canada, where she is currently an University Professor and an University Research Chair in wireless communication networks. Her current research interests include network architecture, algorithms and protocols, and service provisioning in future communication systems. She is a fellow of the Royal Society of Canada (RSC), Canadian Academy of Engineering (CAE), and the Engineering Institute of Canada (EIC). She is an elected member of the Board of Governors (BoG) of the IEEE Vehicular Technology Society (VTS). She was a recipient of the Technical Recognition Award in Ad Hoc and Sensor Networks in 2017 from the IEEE Communications Society, the Women's Distinguished Career Award in 2021 from the IEEE Vehicular Technology Society, the R. A. Fessenden Award in 2021 from IEEE Canada, and the Award of Merit in 2021 from the Federation of Chinese Canadian Professionals (Ontario). She was the VTS President (2023–2024) and the Editor-in-Chief of IEEE TRANSACTIONS ON VEHICULAR TECHNOLOGY (2007–2013), an Editor of IEEE TRANSACTIONS ON WIRELESS COMMUNICATIONS (2005–2009), and an IEEE Communications Society Distinguished Lecturer (2008–2011).

Xuemin (Sherman) Shen (Fellow, IEEE) received the Ph.D. degree in electrical engineering from Rutgers University, New Brunswick, NJ, USA, in 1990.

He is currently an University Professor with the Department of Electrical and Computer Engineering, University of Waterloo, Canada. His research focuses on network resource management, wireless network security, the Internet of Things, 5G and beyond, and vehicular networks.

Dr. Shen is a registered Professional Engineer of Ontario, Canada, an Engineering Institute of Canada Fellow, a Canadian Academy of Engineering Fellow, a Royal Society of Canada Fellow, a Chinese Academy of Engineering Foreign Member, and an International Fellow of the Engineering Academy of Japan. He is the Past President of the IEEE ComSoc, the Vice President for Technical & Educational Activities, the Vice President for Publications, and a Member-at-Large on the Board of Governors. He has also received Premier's Research Excellence Award (PREA) in 2003 from the Province of Ontario, Canada, and the Excellent Graduate Supervision Award in 2006 from the University of Waterloo. He received Joseph LoCicero Award in 2015 and Education Award in 2017 from the IEEE Communications Society (ComSoc), Technical Recognition Award from Wireless Communications Technical Committee in 2019 and AHSN Technical Committee in 2013, James Evans Avant Garde Award in 2018 from the IEEE Vehicular Technology Society, the R. A. Fessenden Award in 2019 from IEEE, Canada, Award of Merit from the Federation of Chinese Canadian Professionals (Ontario) in 2019, Canadian Award for Telecommunications Research from the Canadian Society of Information Theory (CSIT) in 2021, President's Excellence in Research from the University of Waterloo in 2022, and "West Lake Friendship Award" from Zhejiang Province in 2023. He serves/served as the General Chair for the 6G Global Conference'23 and ACM Mobihoc'15; the Technical Program Committee Chair/Co-Chair for IEEE Globecom 2007, 2016, and 2024, IEEE Infocom'14, and IEEE VTC'10 Fall; and the Chair for the IEEE ComSoc Technical Committee on Wireless Communications. He served as the Editor-in-Chief for the IEEE INTERNET OF THINGS JOURNAL, *IEEE Network*, and *IET Communications*.